

¹ **Stratospheric Variability and Tropospheric**
² **Ozone**

Juno Hsu and Michael J. Prather

Juno Hsu, Earth System Science, University of California, Irvine. 92697. Email: junoh@uci.edu

¹Earth System Science, University of
California, Irvine, California, USA

Abstract. Changes in the stratosphere-troposphere exchange (STE) of ozone over the last few decades have altered the tropospheric ozone abundance, and are likely to continue doing so in coming century as climate changes. Combining an updated linearized stratospheric ozone chemistry (Linoz v2) with parameterized Polar Stratospheric Clouds (PSCs) chemistry, a five-year (2001-2005) sequence of European Centre for Medium-Range Weather Forecasts (ECMWF) meteorology data, and the UCI chemistry transport model (CTM), we examine variations in STE O_3 flux and how it perturbs tropospheric O_3 . Our estimate for the current STE ozone flux is 290 Tg/yr in the Northern Hemisphere (NH) and 225 Tg/yr in the Southern Hemisphere (SH). The 2001-2005 interannual rms variability is 25 Tg/year for the NH and 30 Tg/year for the SH. STE drives a seasonal peak-to-peak NH variability in tropospheric ozone of about 7-8 DU. Of the interannual STE variance, 20% and 45% can be explained by the quasi-biennial oscillation (QBO) in the NH and SH respectively. The CTM matches the observed QBO variations in total column ozone and STE O_3 flux shows negative anomalies over the mid-latitudes during the easterly phases of the QBO. When the observed column ozone depletion from 1979 to 2004 is modeled with Linoz v2, we predict STE reductions of at most 10 % in NH, corresponding to a mean decrease of 1 ppb in tropospheric O_3 .

1. Introduction

3 Scientific efforts to understand the trends and variations in ozone observed over the
4 past few decades have demonstrated the role of both photochemical and meteorological
5 factors in driving stratospheric ozone change (e.g., Randel and Wu, 2007; Stolarski et
6 al., 2006, Salawitch et al., 2005). It has been proposed that these stratospheric changes
7 have altered the tropospheric ozone burden over the past few decades (Fusco and Lo-
8 gan, 2003) and will continue to affect it in the future (Sudo et al., 2003). This paper
9 presents a series of highly constrained modeling experiments that capture the observed
10 trends and variations in stratospheric ozone and diagnose the corresponding changes in
11 the stratosphere-to-troposphere flux of ozone. We are thus able to better understand the
12 seasonal, interannual, and decadal trends in tropospheric ozone and the oxidative capacity
13 of the lower atmosphere as driven by the stratosphere.

14 The coupling of stratospheric and tropospheric ozone with chemistry models or with
15 chemistry-climate models is occurring across the community (Eyring et al., 2005). These
16 full models include a nearly complete set of chemical species and reactions that affect
17 ozone, but are costly to run, and are often difficult to diagnose as to the causative fac-
18 tors of variability. We approach the problem with a simplified chemical model that is
19 focused on simulating the stratosphere-to-troposphere exchange (STE) of ozone: a lin-
20 earized ozone chemistry (Linoz version 1: McLinden et al., 2000) combined with unique
21 transport diagnostics that quantify the STE ozone flux as a function of time and place
22 (Hsu et al., 2005). The Linoz model is revised (Section 2) to use updated climatologies
23 for background stratospheric composition and current photochemical data (IUPAC, 2004;
24 Sander et al., 2006). Stratospheric ozone simulated with the new Linoz version 2 in the

University of California, Irvine (UCI) Chemistry Transport Model (CTM) driven by Oslo
ECMWF Integrated Forecast System (IFS) meteorology data is tested against observed
ozone climatology (Section 3). The seasonal and interannual relationship between strato-
spheric ozone, STE ozone flux, and tropospheric ozone is derived for a continuous sequence
of meteorological fields from January 2000 to December 2005 (Section 4). The extent of
the halogen-driven ozone STE decrease since 1979 is derived (Section 5), and we discuss
the overall role of the stratosphere in driving tropospheric ozone change (Section 6).

We find that stratosphere alone produces a peak-to-peak seasonal variation in tro-
pospheric column ozone of about 7-8 DU at northern mid-latitudes that parallels the
late summer maximum normally attributed to tropospheric photochemistry. The Quasi-
Biennial Oscillation (QBO) signature in total column ozone roughly matches that ob-
served, and the QBO signals in STE ozone flux have maximum amplitudes in midlati-
tudes that are opposite in phase to its midlatitude QBO signal in total column ozone. The
observed, post-1979 ozone depletion for the NH can be best simulated in the UCI CTM
with a 4K higher threshold activation temperature than the typical 195K threshold for
PSC formation. Enhanced background bromine levels are found to have negligible effect
on ozone depletion but our PSC chemistry is parameterized for fixed bromine and so only
our non-PSC chemistry responds to enhanced Br_y . The maximum simulated decrease
in the STE flux for post-1979 ozone depletion is about 10% in the NH and 22% in the
SH. Furthermore, the latitude-season pattern of STE decrease due to ozone depletion is
distinctly different from the pattern of change in total column ozone.

2. A linearized stratospheric Ozone Chemistry – Linoz version 2

46 Linoz is linearized ozone chemistry for stratospheric modeling (McLinden et al., 2000).
 47 It calculates the net production of ozone (i.e. production minus loss) as a function of
 48 only three independent variables: local ozone concentration, temperature, and overhead
 49 column ozone). A zonal mean climatology for these three variables as well as the other
 50 key chemical variables such a total odd-nitrogen methane abundance is developed from
 51 satellite and other in situ observations. A relatively complete photochemical box model
 52 (Prather, 1992) is used to integrate the radicals to a steady-state balance and then com-
 53 pute the net production of ozone. Small perturbations about the chemical climatology
 54 are used to calculate the coefficients of the first-order Taylor series expansion of the net
 55 production in terms of local ozone mixing ratio (f), temperature (T), and overhead column
 56 ozone (c),

$$\frac{df}{dt} = (P - L)^o + \left. \frac{\partial(P - L)}{\partial f} \right|_o (f - f^o) + \left. \frac{\partial(P - L)}{\partial T} \right|_o (T - T^o) + \left. \frac{\partial(P - L)}{\partial c} \right|_o (c - c^o). \quad (1)$$

57 The photochemical tendency for the climatology is denoted by $(P-L)^o$, and the climatology
 58 values for the independent variables are denoted by f^o , c^o , and T^o , respectively. Including
 59 these four climatology values and the three partial derivatives, Linoz is defined by seven
 60 tables. Each table is specified by 216 atmospheric profiles: 12 months by 18 latitudes (85S
 61 to 85N). For each profile, quantities are evaluated at every 2 km in pressure altitude from
 62 $z^* = 10$ to 58 km ($z^* = 16 \text{ km} \log_{10} (1000/p)$). These tables are automatically remapped
 63 onto any CTM grid with the mean vertical properties for each CTM level calculated as
 64 the mass-weighted average of the interpolated Linoz profiles. Equation 1 is implemented
 65 for the chemical tendency in the CTM.

66 We adopt the ozone climatology compiled by McPeters et al. (2007) which has improved
67 profiles over the tropics and the SH from recent balloon sonde measurements from the
68 Southern Hemisphere Additional Ozonesondes program. The temperature climatology
69 is unchanged (Nagatani and Rosenfield, 1993). The remaining chemical composition is
70 specified as a climatology scaled to the tropospheric abundance of the long-lived source
71 gases (i.e., N_2O , CH_4 , and the halocarbons) so that it can be changed to reflect a changing
72 atmosphere. This includes climatologies for three chemical families ($\text{NO}_y = \text{NO} + \text{NO}_2$
73 + HNO_3 + ...; $\text{Cl}_y = \text{ClO} + \text{HOCl} + \text{ClONO}_2 + \text{HCl} + \dots$; $\text{Br}_y = \text{Br} + \text{BrO} + \text{BrONO}_2$
74 + ...). We use N_2O as the primary measure of stratospheric composition and tracer-tracer
75 relations to define the other trace gases. A monthly, latitude-by-height N_2O climatology
76 above 22 km is based on CLAES satellite measurements (Oct 1991- May 1993, Randel
77 et al., 1994) and below 22 km is constructed from the compact correlation with O_3 from
78 the NASA ER-2 in-situ measurements in the lower stratosphere (Strahan et al., 1999).
79 The CH_4 and NO_y distributions are obtained using the polynomial fit with respect to
80 N_2O from ATMOS measurements (Michaelson et al., 1998a; 1998b). The Cl_y climatology
81 assumes conservation of halogens, thus increasing in the stratosphere as the organic source
82 gases (e.g., CFCs, CH_3CCl_3 , CCl_4) are photochemically destroyed (Woodbridge et al.,
83 1995). The Br_y climatology likewise assumes increasing Br_y as the tropospheric bromine
84 source gases (e.g., CH_3Br , CF_2BrCl , CF_3Br) are destroyed (Wamsley et al., 1998). For
85 Br_y , we consider a sensitivity case where the tropopause value is increased to 6 ppt
86 to include the relatively large amounts of inorganic bromine (Br_y) that may cross the
87 tropopause (Salawitch et al., 2005). Water vapor adopts a lower boundary fixed at 3.65
88 ppm and follows conservation of potential water ($\text{H}_2\text{O} + 2x\text{CH}_4 = \text{constant}$) throughout

89 the stratosphere (Nassar et al., 2005). The tracer-tracer correlations are applied with N_2O
90 scaled to the year of their observed correlations. Normalized distribution patterns for
91 N_2O , CH_4 , H_2O , NO_y and Br_y in January are shown in Fig. 1. Tracer-tracer correlations
92 derived from the more modern and complete observations yield trace gas distributions
93 that are much improved compared with the ones used in the older version of Linoz.

94 Ozone and temperature climatologies, to first order, determine stratospheric photolysis
95 rates. We adopt a surface reflectivity of 0.3 as an average cloud cover. The photochem-
96 ical box model is initialized with an approximate balance of species within each of the
97 chemical families and integrated for 30 days to reach an approximate, diurnally repeat-
98 ing steady state, whereby the initialization of species within the families is, for the most
99 part, forgotten. During this integration, the abundance of ozone and long-lived gases
100 are fixed, and the chemical families are conserved. The net ozone production and three
101 partial derivatives are evaluated numerically by perturbing the local ozone by +5%, the
102 overhead column ozone by +5%, and the temperature by +4 K. The second-order terms
103 in the Taylor expansion (equation 1) are negligible for reasonable perturbations about the
104 climatology (see Figure 3 of McLinden et al., 2000).

105 For Linoz version 2, the photochemistry has been updated from the 1997 -vintage version
106 1 to current rate coefficients (Sander et al., 2006) and cross sections (IUPAC, 2004). New
107 solar fluxes are taken from the average solar irradiance reference spectra derived by the
108 SUSIM team for two different levels of solar activity (Thuillier et al., 2004). Compared
109 to Linoz v1, these are 15-20 % larger at wavelengths 177-200 nm, 5-10% larger at 200-300
110 nm, but relatively unchanged at wavelengths longer than 300 nm. Other notable updates

111 affecting photolysis rates include the quantum yield of $O(^1D)$ from O_3 photolysis and the
112 NO_2 cross sections.

113 As an example of how the stratospheric chemistry model has evolved since v1, we follow
114 the chemistry updates using a standard ATMOS profile (May 31, 30N) from previous
115 models and measurements studies (Prather and Remsberg, 1993). The height profiles
116 of net ozone production (P-L) and its derivatives with respect to ozone, temperature,
117 and overhead column ozone are shown in Fig. 2. A sequence of six model calculations
118 are shown with successive updates tracking the change in chemistry from Linoz v1 to
119 v2. Values generated with the JPL-1997 kinetics rates and cross sections and with the
120 old solar flux data used for generating Linoz v1 are shown for comparison (JPL97-S3).
121 Updating the quantum yields and cross sections only (JPL97-S2) has no effect on the three
122 derivatives and a barely noticeable effect on net production, i.e., a small increase near 40
123 km. Updating the solar fluxes in addition (JPL97-S1) also has no effect on the derivatives
124 but causes a large increase in net production throughout the stratosphere above 25 km.
125 The update to JPL 2000 kinetics (JPL00-S1) causes a notable decrease in the temperature
126 derivative between 34 and 48 km with an increase in net production from 34 to 44 km and
127 a decrease below 34 km. Updating the kinetics to JPL 2002 (JPL02-S1) and JPL 2006
128 (JPL06-S1) has minor effects, with the latter causing a small decrease in net production
129 about 30 km.

130 The largest and most extensive changes in the chemical model occur in the net ozone
131 production and not in the derivatives. The largest change in updating from JPL 1997
132 to JPL 2000 is caused by the addition of a new branch for the reaction, $OH + ClO \rightarrow$
133 $HCl + O_2$. This new pathway weakens the Cl_y -catalyzed ozone loss and thus results in

134 an increase in net production peaking around 38 km. The other major change with JPL
135 2000 kinetics was a stronger NO_y -catalyzed ozone loss from the increased kinetic rate for
136 the reaction, $\text{NO}_2 + \text{O} \rightarrow \text{NO} + \text{O}_2$, and decreased kinetic rate for the reaction, $\text{NO}_2 +$
137 $\text{OH} \rightarrow \text{HNO}_3$. Changes to chemical reaction rates after JPL 2000 have relatively minor
138 effects on the ozone chemistry (outside of PSC conditions).

139 Linoz v1 considered only non-PSC chemistry and did not include chlorine activation by
140 Polar Stratospheric Clouds (PSCs). Thus, in v1 there was no Antarctic ozone hole and no
141 enhanced Arctic loss during cold winters. In v2, we incorporate the PSC parameterization
142 scheme of Cariolle et al. (1990) when the temperature falls below 195 K and the sun is
143 above the horizon at stratospheric altitudes. The O_3 loss scales as the squared strato-
144 spheric chlorine loading (normalized by the 1980 level threshold). In this formulation PSC
145 activation invokes a rapid e-fold of O_3 based on a photochemical model, but only when
146 the temperature stays below the PSC threshold. It does not consider that the activated
147 chlorine continues to destroy ozone for several days after encountering a PSC (Schoeberl
148 et al., 1993). Recently, Cariolle and Teyssedre (2007) added a cold-tracer to account for
149 this effect. Their new parameterization, which is not used here, will be more important in
150 the Arctic where PSCs are not sustained throughout the winter. In view of this process
151 and the evidence of Cl_y activation on ternary aerosols at warmer temperatures (Thornton
152 et al., 2005), we test another version using a higher PSC-activation temperature of 199K.

153 Linoz chemical tendencies are applied only in the stratosphere, defined here as CTM grid
154 points for which the O_3 abundance is greater than 100 ppb (10^{-7} moles per mole of dry air).
155 These simulations do not include realistic tropospheric ozone chemistry, but instead invoke
156 a parameterized sink that restores O_3 to 20 ppb in the lowest 600 m of the troposphere

157 with an e-folding time-scale of 2 days (Hsu et al., 2005). The choice of 20 ppb was made
158 to imitate a more realistic chemistry and produce reasonable tropospheric column O_3 .
159 This tropospheric pseudo-chemistry is uniform, and thus variations in tropospheric O_3
160 calculated here are driven entirely by the STE ozone flux. When combining Linoz with
161 a full tropospheric chemistry model, we simulate a separate Linoz tracer (O_{3s}) and use
162 it every time step in each grid box to determine if the tropospheric chemistry is invoked
163 (e.g., $O_{3s} < 100$ ppb) or if the Linoz net chemical tendencies are used ($O_{3s} > 100$ ppb).

164 Using the normalized, monthly 2-D climatologies for stratospheric composition, we cal-
165 culate five sets of Linoz v2 tables (see Table 1). Linoz-1979 uses the 1979 mean abundances
166 from REF 1 of Eyring et al. (2005) and represents a stratosphere prior to significant
167 ozone depletion. With Cl_y levels below the chlorine-loading threshold, PSC-induced loss
168 is never invoked with Linoz-1979. Linoz-2004 uses year-2004 mean tropospheric abun-
169 dances (WMO, 2006, Table 1-2) and generates an Antarctic ozone hole. A second pair
170 of Linoz tables, -1979Br and -2004Br, assume a 6ppt greater background of Br_y through-
171 out the stratosphere (see Salawitch et al., 2005). We also use the Linoz-2004Br tables
172 with a warmer PSC threshold of 199K and denote this case as Linoz-2004BrT. Note that
173 the Linoz tables assume only gas phase chemistry plus some sulfate reactions ($N_2O_5 +$
174 aerosol, $BrONO_2 +$ aerosol) using year 1990 of the SAGE II climatology (Thomason et
175 al., 1997) for the aerosol surface area. Without very cold, ternary-aerosol chemistry, ClO
176 levels in the lower stratosphere are always low and the additional background Br_y does
177 not notably enhance ozone loss.

3. Evaluating Column Ozone with Linoz

178 To assess the impact of the updated Linoz v2 on stratospheric ozone, we repeat the
179 Linoz v1 simulations of Hsu et al. (2005) with Linoz-2004 and the Oslo/EC meteorology
180 for year 1997 derived from the ECMWF IFS Cycle 23r4. Linoz v1 is known to be biased
181 low in column O_3 in the tropics and high in high latitudes (see Fig. 1 of Wild et al.,
182 2003). With Linoz-2004 this bias is mostly eliminated: tropical ozone columns increase
183 by 5-20% for all but the northern winter, and outside of the tropics ozone is reduced by
184 similar percentages for all months except December. In terms of STE, if we run Linoz-
185 2004 tables but turn off the PSC parameterization, the O_3 flux increases by 9% from 516
186 Tg/yr (Linoz v1 tables) to 563 Tg/yr, with greater increases in the SH. The spatial and
187 temporal STE patterns remain roughly the same. Inclusion of the parameterized PSC
188 chemistry with Linoz-2004 reduces the STE ozone fluxes globally by 10%, again with
189 greater response in the SH. The total shift in STE ozone flux from v1 to v2 (Linoz-2004)
190 is +3% in the NH and -7% in the SH. Thus, the changes in the photochemical data and
191 inclusion of a parameterized PSC loss have corrected the prominent biases in Linoz v1
192 but the total STE ozone flux is only slightly reduced.

193 Stratospheric column O_3 calculated with Linoz-2004 with 1997 ECMWF IFS Cycle23r4
194 meteorological data are compared with those from observations (McPeters et al., 1997;
195 2007) in Fig. 3. We show results for both with and without PSC parameterization. For
196 both CTM and observations, the stratosphere is defined as where O_3 abundances exceed
197 100 ppb. The observed climatology compiled by McPeters et al. (2007) is an improvement
198 over the climatology compiled by McPeters et al. (1997), but the changes also reflect the
199 inclusion of more recent years with greater ozone depletion, e.g., a deeper Antarctic ozone

200 hole in September and greater Arctic loss in March. From 40S to 40N, the Linoz simulation
201 is excellent, with no obvious biases and errors less than 25 DU. At high latitudes, the PSC
202 parameterization in general improves the Linoz simulations, particularly for the SH ozone
203 hole. However, the model-climatology comparison in Fig. 3 looks bad in polar regions for
204 some months, due in part to the circulation (e.g., the model's seasonal recovery from the
205 Antarctic ozone hole is too rapid) and in part to the observations being extrapolated (e.g.,
206 70-90 N in December). The comparison is also for only one year of EC meteorology and
207 a better comparison of the seasonality in total column O₃ is presented in Fig. 4 below.

208 To study interannual variability we use continuous ECMWF IFS T42L40 meteorological
209 fields from years 2000 through 2005. Year 2000 data are extracted from ECMWF IFS
210 Cycle 23r4 model whereas the rest are extracted from Cycle 29r2 model. We find Cycle
211 29r2 generates about 20% more STE flux than does version Cycle 23r4 (see below), and this
212 difference is much greater than the interannual variability. Thus, year 2000 meteorological
213 data are only used to spin up the experiments to approach a steady state before continuing
214 with the next five years from January 2001 through December 2005, which are analyzed
215 here. This five-year monthly mean climatology of total column O₃, plus the interannual
216 variability defined relative to the five-year mean, are compared with the recent corrected
217 Earth Probe TOMS observations based on NOAA-16 SBUV/2 ozone records as shown
218 in Fig. 4. Note that the missing data for December 2005 are replaced with those from
219 December 2004 for convenience. This CTM simulation with Linoz-2004 captures the
220 general patterns of the observed seasonal cycle and the Antarctic ozone hole with its
221 minimum below 190 DU. At mid and high northern latitudes, total column O₃ is well
222 simulated. In the tropics, the minimum (NDJF at 15N) are likewise matched, but the

223 CTM has a spurious high (310 DU contour) in July at 10N and likewise with 270 DU
224 contour bulging equatorward to 10S in austral summer. Even worse, the circum-Antarctic
225 maximum around 60S is consistently about 60 DU higher than observed. These anomalies
226 do not appear in the previous publications with Linoz v1 using the 1997 and 2000-2001
227 Cycle 23r4 meteorological data. Using Linoz-2004BrT reduces the total ozone error by 20
228 DU confined to poleward of 60S and over the spring Arctic vortex. The spurious errors
229 remain evident and large regardless of the chemistry used.

230 Analysis of the monthly latitude-height ozone profiles from the CTM (not shown) reveals
231 a deep sinking motion near the edge of the Antarctic polar vortex that persists through the
232 seasons and a spurious downward shift of contours in the top model layers at 10N in July
233 and 10S in January. We presume these errors stem from a poorly resolved stratosphere
234 with a top lid in the middle stratosphere (2 hPa). To test this point, we acquired year
235 2005 using IFS Cycle 29r2 but with much finer vertical resolution, T42L60, in which
236 the whole stratosphere is resolved with layers at most 1.5 km thick from 15 to 0.5 hPa.
237 Linoz-2004 with the T42L60 meteorological data corrects the worst errors seen with the
238 T42L40 meteorological data as shown in Fig. 5, viz, the tropical bubble disappears and the
239 circum-Antarctic high columns now are lower and closer to observations. Unfortunately,
240 the T42L60 data was only available to us for year 2005, and so our analysis of interannual
241 variability continues with the T42L40 data.

242 Monthly anomalies in zonal-mean total column O_3 for years 2001-2005 are shown in
243 Fig. 4c and 4d. In October 2002, the CTM matches the extremely high column anomaly
244 over Antarctica, which was caused by a sudden warming event and the transport of ozone-
245 rich air into the vortex (e.g. Simmons et al., 2005). In general the phases of alternating

246 high and low anomalies are well captured by the CTM and a two-year QBO-like signal
247 is evident. In spite of the coarsely resolved lower stratosphere, the ECMWF IFS 40-
248 layer model produces a QBO with alternating descending easterlies and westerlies in the
249 stratosphere (not shown). The forecast model is re-initialized with observations every
250 24 hours and appears to generate a QBO pattern in the lower stratospheric transport.
251 The magnitude of the modeled equatorial and SH interannual variability in O_3 column,
252 however, is often twice as large as observed.

253 To understand the modeled interannual variability and its relation to the STE O_3 flux,
254 we isolate the QBO signal following the regression procedure of Randel and Wu (1996). A
255 QBO time series is defined by determining the linear combination of the equatorial zonal
256 wind at 20 and 40 hPa that best correlates the equatorial total column O_3 interannual
257 variability. This time series is then regressed against the time series of total column
258 O_3 anomalies at all latitudes (Fig 4d). Fig. 6 shows (a) the modeled total column O_3
259 anomalies associated with the QBO and (b) the residuals. The QBO signal in total column
260 O_3 shows large positive (negative) equatorial ozone anomalies during equatorial westerlies
261 (easterlies) as observed. The subtropical QBO signal is correctly out-of-phase with the
262 equatorial signal. However, this signal is more confined to the subtropics than is observed
263 (see Fig. 1 of Randel and Wu, 1996), and the observed 6-month phase lag between the
264 maxima at subtropical and mid latitudes in the two hemispheres is absent. Also unlike
265 earlier observations (e.g. Randel and Cobb 1994), the SH midlatitude QBO signal does
266 not continue into to the spring Antarctic polar region but directly changes sign before 60S.
267 This points to the possibility that for the coarsely resolved stratosphere of the ECMWF
268 L40 model, the interaction of the annual cycles and the QBO as well as the high-latitude

269 planetary waves modulated by the QBO (See Baldwin et al., 2001) are completely missing
270 or even misrepresented. The residuals are about the same magnitude as the QBO signal
271 and show a large-scale, low-frequency, coherent structure in the SH that is roughly out of
272 phase with the structure at the equator.

4. STE Ozone Flux and Tropospheric Ozone

273 Following Hsu et al. (2005), the STE ozone flux is calculated based on the mass balance
274 of each latitude-by-longitude tropospheric ozone column on the CTM grid points. The
275 net STE ozone flux is the residual from three terms computed hourly: the change in
276 tropospheric ozone mass, the flux divergence of tropospheric ozone (i.e. air mass with
277 abundance < 100 ppb) and the parameterized ozone sink in the lowermost layers. In
278 this study, the diagnostic is further improved by using the first moment of the horizontal
279 ozone flux to determine the fraction of the ozone flux being advected to a neighboring
280 CTM box that is tropospheric (i.e. < 100 ppb) whereas in the previous study only the
281 mean abundance of the advective flux is used. This improvement has greatly reduced the
282 overall noise level such as the dipole structures within the Pacific jet stream noted in the
283 previous study. Figure 7 shows the averaged seasonal cycle of STE O_3 fluxes calculated
284 from the CTM simulations with Linoz-2004 from years 2001-2005 (white contour lines)
285 along with the average zonal-mean zonal wind at 200 hPa (shaded contours). Similar to
286 the year 1997 and 2000/2001 results (Figure 10 of Hsu et al., 2005), the STE maximum
287 in the NH occurs just poleward of the tropospheric zonal jet, peaks during late spring
288 and early summer when the zonal jet weakens, and migrates with the subtropical jet up
289 to 45N. In the SH, the STE maximum stays around 30S, does not migrate poleward with
290 the jet in summer, but does peak during austral spring when the jet weakens. However,

291 the global STE flux is on average 20 % larger than the previous estimates (Hsu et al.,
292 2005) despite the fact that as discussed in Section 3, the global STE flux should be
293 slightly reduced using Linoz-2004 and including the PSC parameterization. The larger
294 magnitude is mostly due to the excessive descent in the Antarctic circumpolar region with
295 the Cyc29r2 L40 fields as already seen in total column ozone discussed above. Indeed,
296 recalculating the STE flux using the ECMWF 2005 Cyc29r2 L60 data, we find that the
297 L40 SH STE flux is about 25 % too large.

298 The QBOs role in modulating the STE O_3 flux is derived with the same method as for
299 total column O_3 . STE variability attributed to the QBO (Fig. 6c) is small: peak contour
300 intervals in mid-latitudes are $+0.20 \text{ g m}^{-2} \text{ yr}^{-1}$ (30S in 2004) as compared with a global
301 average of about $1.2 \text{ g m}^{-2} \text{ yr}^{-1}$ (i.e., 610 Tg per year). These mid-latitude STE QBO
302 signals are out of phase with the mid-latitude total column ozone QBO, and, not sur-
303 prisingly, there are no QBO signals over the tropics and high latitudes where STE ozone
304 fluxes are negligible. This pattern indicates that the induced sinking part of the overturn-
305 ing circulation in the subtropics during the easterly phase of QBO creates a dynamical
306 condition that disfavors the mixing of the mid-latitude, lower stratospheric ozone into the
307 troposphere. The STE residual field (Fig. 6d) has much larger amplitudes than the QBO
308 signal. In SH both STE and total column O_3 residuals show the same low-frequency vari-
309 ability. At 35S, they are positively correlated with a maximum correlation coefficient 0.44
310 with STE lagging total column ozone residual by 9 months. This relationship is mostly
311 evident between the positive total column ozone anomaly in June 2003 (red patch, Fig.
312 6b) followed by the positive STE anomaly (red patch, Fig. 6d) in early 2004. However, a

313 longer data set will be needed to confirm its significance. In the NH, the STE residuals
314 lack coherence and have smaller amplitudes.

315 Influx of O_3 from the stratosphere is a principal component of the tropospheric O_3
316 budget, the others being in situ photochemical production and loss and surface deposition.
317 The amount of tropospheric O_3 that can be assigned a stratospheric origin, however, is
318 not well defined. There is a wide range of reported STE fluxes and various accounting
319 methods for tropospheric production and loss (e.g., Prather et al., 2001; Stevenson et al.,
320 2006). In this study, we quantify the variability in tropospheric O_3 caused by changes in
321 STE by using a simplified, uniform chemistry in the troposphere, viz, O_3 in the lowest
322 600m is relaxed towards 20 ppb. We diagnose tropospheric column O_3 (adopting common
323 usage of TCO for the tropospheric column ozone) hourly as the vertically integrated
324 ozone burden for all CTM layers with abundances less than 100 ppb. Thus, with these
325 simulations, the latitudinal and seasonal variations in TCO (color-filled contours in Fig.
326 8a) are driven by STE ozone flux (line contours in Fig. 8a). In the NH, the monthly
327 zonal-mean TCO varies from 16 to 26 DU with lowest values in the tropics (where the
328 troposphere is largest). In northern mid-latitudes, the seasonal peak-to-peak range is 8
329 DU, and although this tends to follow the troposphere mass (i.e., the tropopause peaks in
330 late summer) a large fraction appears to follow the STE ozone flux. This large seasonality
331 is driven without tropospheric chemistry. We expect the TCO to lag the STE by a month
332 (i.e., the tropospheric lifetime of an STE perturbation, see Section 6 for more discussion).

333 Comparing to the recently observed TCO derived from OMI and MLS measurements
334 (Fig. 6 of Ziemke et al, 2006), our modelled TCO without tropospheric chemistry surpris-
335 ingly matches the observed latitude-by-month pattern, much better than the comparison

336 with the full chemistry CTM in Ziemke et al. Our TCO is, however, consistently biased
337 low by about 8 DU over the tropics and wintertime mid-latitudes. Furthermore, we un-
338 derestimate the magnitude of the buildup to maximum TCO seen at 40N in July and
339 at 30S in November by 18 DU, indicating the importance of tropospheric photochemical
340 net production that is not simulated here. Renormalizing the TCO pattern to the tropo-
341 spheric mass shows the variation in mean tropospheric ozone abundance (ppb in Fig. 8b).
342 Here, we see that peak abundances tend to follow the STE ozone flux. Given that the
343 tropospheric parameterization pushes to a uniform mixing ratio, this simulation provides
344 a measure of the seasonality and amplitude of tropospheric O₃ variability driven by STE.

5. Ozone Depletion and STE Ozone fluxes

345 The reduction in STE O₃ flux from the halogen-catalyzed depletion of stratospheric O₃
346 is evaluated with different Linoz v2 models. We simulate pre-depletion O₃ with Linoz-1979
347 using the meteorological data for years 2001-2005. For post-depletion, we use the same
348 meteorological data and Linoz-2004. Additional experiments, Linoz-2004Br and Linoz-
349 2004BrT are used to investigate the effect of enhanced bromine background and higher
350 PSC temperature threshold for post-ozone depletion. Because the additional bromine rep-
351 resents a natural tropospheric source, we simulate the pre-depletion ozone, Linoz-1979Br
352 to be paired with the latter experiments. Note that because we have only meteorological
353 data for recent years, this study cannot elucidate the role of changing transport in the
354 observed depletion.

355 All three Linoz variants (2004 vs 1979, 2004Br vs 1979Br and 2004BrT vs 1979Br)
356 calculate qualitatively similar latitudinal patterns of column O₃ depletion as observed
357 in the merged satellite data based on TOMS/SBUV measurements from 1979-2000, e.g.,

358 maximum NH spring depletion of about 6% per decade in the polar region (Figure 11 of
359 Fioletov et al. 2002). All Linoz simulations show largest depletion in spring and in winter
360 over the polar region of each hemisphere. However, the magnitude of the overall ozone
361 depletion and the difference between the strong spring/winter depletion and the weak
362 fall/summer depletion in the NH, are largely underestimated unless the activation tem-
363 perature of the PSC parameterization is raised from 195K to 199K. Additional bromine
364 background has only a small effect on further ozone depletion in these calculations com-
365 pared to Salawitch et al. (2005). As noted before, we speculate that this could be the
366 result of our PSC parameterized loss being independent of bromine level.

367 Fig. 9 shows the latitude-by-month changes in total column O_3 (DU) and STE O_3
368 flux ($g\ m^{-2}\ yr^{-1}$) between Linoz-1979Br and Linoz-2004BrT for the five year average of
369 2001-2005 meteorology. We can compare the ozone depletion in Fig. 9a directly to the
370 vertically integrated SAGE/sonde stratospheric ozone data over 1979-2005 (Fig. 10 of
371 Randel and Wu, 2007). Overall, the simulations agree with observations, both in shape
372 and magnitude. In the tropics, the difference of about 8 DU in total column O_3 relative
373 to the pre-ozone depletion is as large as seen in SAGE/sonde data (Fig. 10a of Randel
374 and Wu, 2007), but disagrees with the equatorial total ozone change of about zero seen in
375 the merged TOMS/SBUV data (Fig. 10b of Randel and Wu, 2007). In our simulation at
376 T42L40, the top layer from 2 to 20 hPa does not accurately cover the diversity in upper
377 stratospheric O_3 chemistry whereby chlorine-driven depletion above 3 hPa results in more
378 penetration of solar ultraviolet and hence more O_3 production below. Other errors in our
379 simulation include: missing the second maximum in NH ozone depletion during the fall;
380 and simulating Antarctic ozone depletion to be about twice as large as the observed. The

381 latter discrepancy could be reduced if there were some PSC-induced ozone loss already in
382 1979, which is not modeled here.

383 The latitude-month change in the STE ozone flux is quite different from that in total
384 column ozone. For the NH STE change, the difference pattern follows roughly the seasonal
385 pattern in Fig. 7 but with the maximum depletion in summer lagging the seasonal STE
386 maximum by 2 months. The maximum change in the NH STE ozone fluxes is about
387 $-0.3 \text{ g m}^{-2} \text{ yr}^{-1}$ (less than 10 % change) and is about twice that obtained when the PSC
388 threshold is lowered to 195 K. The SH STE change pattern does not resemble its seasonal
389 pattern. The maximum decrease, $-0.7 \text{ g m}^{-2} \text{ yr}^{-1}$, occurs in the austral summer around
390 40S with a six month time-lag from the Antarctic ozone hole. Antarctic ozone, primarily
391 in the isolated vortex, requires more time to propagate to the midlatitudes than its NH
392 counterpart.

393 Fig. 10 shows the seasonal changes in the ozone vertical profiles at NH mid latitudes
394 for all three pairs of experiments. Decreases are most evident near 11-14 km in the lower
395 stratosphere as the peak moves down in height from spring to summer. The annual
396 maximum decrease in the lower stratosphere from Linoz-2004BrT minus its pre-ozone
397 depletion run, Linoz-1979Br, is about 11 %. This trend corresponds to about 8 % per
398 decade for the 1979-1990 period assuming that the total change in ozone between 1979
399 and 2004 is about 1.4 times the linear trend values for 1979-1990 (as stated in Randel and
400 Wu, 2007). It is comparable to the about 7.3 % per decade estimates for a similar period
401 (Randel et al., 1999) but is much smaller than the 30 % decrease, estimate from 1970s to
402 mid 1990s reported in Fusco and Logan (2003). With Linoz-2004Br minus Linoz-1979Br,
403 the net ozone depletion is at most 5 %. The relatively uniform and weak decrease in the

404 NH winter seen in Fig. 10 is distinctly different from the profiles of the other seasons
405 and from observations. It might point to the importance of a trend in winter circulation
406 (Hood and Soukharev, 2005) lacking in this study.

6. Discussion and Conclusions

407 To separate changes in STE ozone flux due to ozone depletion from those due to natural
408 variability, we construct a regression model for the hemispheric monthly STE flux from
409 the five-year sequence for each of the Linoz runs. The STE data are fitted to a hemispheric
410 mean, the seasonal harmonics and the three time series of the QBO, the Arctic Oscillation
411 (AO, Thompson and Wallace, 1998) and the El Nino Southern Oscillation (ENSO) index
412 (Ziemke and Chandra, 2003). The fitted mean and the amplitude of the seasonal cycle
413 decrease in response to changes in halogen loading and the PSC chemistry among different
414 Linoz runs. However, the interannual variances are rather insensitive to the chemical
415 change, thus we use the average percentage change from all model runs for describing the
416 interannual variances.

417 The QBO accounts for about 20 % of the NH interannual variances in STE. Including
418 the AO decreases the unexplained interannual variances only by 2-3 %. The total NH
419 interannual variability is about 25 Tg/yr (rms), the same as the long-term change driven
420 by ozone depletion (Linoz-2004BrT minus Linoz-1979Br). Thus, as detection of a NH
421 trend in column ozone is obscured by transport variability (e.g. Stolarski et al, 2006),
422 so is any long-term change in STE flux. The SH STE flux shows quite different modes
423 of variability. For the SH regression model, we replace the AO index with the AAO
424 (Antarctic Oscillation, Thompson and Wallace, 1998) index. The QBO nearly captures
425 about 45 % of the interannual variability, while the AAO captures negligible variance

426 and thus does not contribute to coherent structure of the residuals seen in Fig. 6d.
427 The maximum SH STE trend due to ozone depletion (70 Tg/yr) is twice as large as the
428 interannual variability (30 Tg/year rms) over the years 2001-2005. Including the ENSO
429 index in either hemisphere does not decrease the unexplained interannual variances. In
430 our model the deseasonalized ENSO index correlates poorly with either hemispheric STE
431 or global STE anomalies in lagged correlations between ± 6 months. The correlation
432 remains poor even after we remove the influence of the QBO from the STE time series.
433 The 2002-2003 El-Nino is readily apparent in our ECMWF meteorological fields but does
434 not enhance the STE O_3 flux in our model. In contrast, Zeng and Pyle (2005) found a
435 high anticorrelation between ozone STE anomalies and the ENSO index six month earlier
436 from 1990-2001.

437 The impact of changes in the STE flux on tropospheric ozone is shown with the scatter
438 plot of the seasonal hemispheric STE fluxes (Tg/year) versus the hemispheric tropospheric
439 ozone burden (Tg) for all 25 years of Linoz v2 simulations for DJF and JJA (Fig. 11).
440 The linear correlations is obvious, particularly for the winter season of each hemisphere.
441 The slope of the scatter plot reflects the lifetime of the perturbations to tropospheric
442 ozone. The NH seasonal lifetime of tropospheric ozone varies from 28-39 days, longest
443 for fall and shortest for spring with an annual mean of 35 days. The lifetimes for the
444 SH have less seasonal variation and are slightly shorter, varying from 27-32 days with an
445 annual mean of 30 days. Our simplified troposphere chemistry allows air of stratospheric
446 origin to wander freely in the troposphere until reaching below 600m altitudes where the
447 O_3 abundance is reset rapidly to 20 ppb. Thus, the lifetime of about one month reflects
448 mostly the characteristics of the tropospheric circulation and mixing and is slightly longer

449 than the estimate of 22 days for all of tropospheric ozone from the multimodel ensemble
450 simulations with full tropospheric chemistry (Stevenson et al., 2006). Realistic loss of
451 stratospheric ozone, occurring throughout the free troposphere, is not simulated in our
452 model. These results, however, will provide a baseline for a corresponding study (in prep)
453 in which the full tropospheric chemistry is included. The intercepts of the scatter plots at
454 zero STE flux reflect our adopted 20-ppb ozone restoring term in the lowermost layers and
455 are higher (in Tg) in summer due to the larger tropospheric volume (higher tropopause).
456 Thus, the total ozone burden and absolute STE ozone flux cannot be used to derive a
457 lifetime.

458 The interannual variability is similar across all model runs regardless of the chemistry,
459 as seen in the similar scatter pattern from each Linoz run. The interannual variability
460 between NH and SH appears uncorrelated. The mean decrease in STE flux due to ozone
461 depletion between Linoz-1979Br and Linoz-2004BrT in the NH is 25 Tg/year, correspond-
462 ing to less than 1 ppb decrease in mean abundance and that in the SH is 72 Tg/year, a
463 2.1 ppb decrease.

464 This study has sought to understand and quantify how the stratosphere influences
465 tropospheric ozone. The scientific results can be summarized as follows:

- 466 • Linoz v2 corrects the low bias in equatorial total column ozone found in Linoz v1,
467 and with ECMWF IFS data our chemistry-transport model better matches the observed
468 stratospheric column ozone.

- 469 • Linoz is useful in diagnosing errors in stratospheric circulation for both general cir-
470 culation models and assimilated winds, e.g., the change in IFS cycle to 29r2 degraded the
471 EC L40 meteorology, but not the L60 version.

472 • Observed interannual variability in total column ozone is well modeled with Linoz
473 and the EC meteorology; however, the modeled magnitude in the SH, including QBO's
474 influence on ozone, is twice as large. Other EC products such as ERA-40 with L60
475 resolution have also shown unrealistic, large SH interannual variability (Fleming et al,
476 2007).

477 • Our best estimate for the current STE ozone flux is 290 Tg/yr in the NH and 225
478 Tg/yr in the SH with interannual variability over years 2001-2005 of ± 25 Tg/year and
479 ± 30 Tg/year respectively.

480 • The STE shows negative anomalies over the mid-latitudes during the easterly phases
481 of the QBO and vice versa. The QBO-induced overturning circulations over mid-latitudes
482 during the easterly phase creates conditions that reduce STE.

483 • The STE flux alone drives a large seasonal change in the tropospheric ozone bur-
484 den with NH mid-latitude peak-to-peak changes of about 7-8 DU that parallels the late
485 summer maximum normally attributed to tropospheric photochemistry.

486 • When the observed column ozone depletion from 1979 to 2004 is modeled with Linoz
487 v2, we predict STE reductions of about 10 %, corresponding to about 1 ppb in tropospheric
488 O₃ of the northern hemisphere, much less than anticipated by Fusco and Logan (2003).

References

489 Baldwin, M. P., et al. (2001), The quasi-biennial oscillation, *Rev. Geophys.*, *39(2)*, 179230.
490 Bojkov, R. D., V. E. Fioletov (1997), Changes of the lower stratospheric ozone over Europe
491 and Canada, *J. Geophys. Res.*, *102(D1)*, 1337-1348, 10.1029/96JD00095.

- 492 Cariolle, D., Lasserre-Bigory, A. and Royer, J. F. (1990), A general circulation model sim-
493 ulation of the springtime antarctic ozone and its impact on mid-latitudes. *J. Geophys.*
494 *Res.*, *95*, 1883-1898.
- 495 Cariolle, D. and H. Teysedre (2007), A revised linear ozone photochemistry parameter-
496 ization for use in transport and general circulation models: multi-annual simulations.
497 *Atmos. Phys. Discuss*, *7*, 1655-1697, 2007.
- 498 Eyring, V., D. E. Kinnison, and T. G. Shepherd (2005), Overview of planned coupled
499 chemistry-climate simulations to support upcoming ozone and climate assessments,
500 *SPARC Newsletter No. 25*, 11-17.
- 501 Fleming, E. L., C. H. Jackman, D. K. Weisenstein, and M. K. W. Ko (2007), The impact
502 of interannual variability on multidecadal total ozone simulations, *J. Geophys. Res.*,
503 *112*, D10310, doi:10.1029/2006JD007953.
- 504 Fusco A. C., J. A. Logan (2003), Analysis of 1970-1995 trends in tropospheric ozone at
505 Northern Hemisphere midlatitudes with the GEOS-CHEM model, *J. Geophys. Res.*,
506 *108 (D15)*, 4449, doi:10.1029/2002JD002742.
- 507 Hsu J., M. J. Prather, O. Wild (2005), Diagnosing the stratosphere-to-troposphere
508 flux of ozone in a chemistry transport model, *J. Geophys. Res.*, *110*, D19305,
509 doi:10.1029/2005JD006045.
- 510 Hood, L.L., and B.E. Soukharev, 2005: Interannual Variations of Total Ozone at Northern
511 Midlatitudes Correlated with Stratospheric EP Flux and Potential Vorticity. *J. Atmos.*
512 *Sci.*, *62*, 37243740.
- 513 IUPAC (2004), International Union of Pure and Applied Chemistry, Subcommittee on Gas
514 Kinetic Data Evaluation, <http://www.iupac-kinetic.ch.cam.ac.uk/>, Datasheets down-

515 loaded 18 May 2004.

516 McPeters, R. D., G. J. Labow, and B. J. Johnson (1997), A satellite-derived ozone clima-
517 tology for balloonsonde estimation of total column ozone, *J. Geophys. Res.*, *102(D7)*,
518 88758886.

519 McPeters R. D., G. J. Labow, J. A. Logan (2007), Ozone climatological profiles for satellite
520 retrieval algorithms, *J. Geophys. Res.*, *112*, D05308, doi:10.1029/2005JD006823.

521 McLinden, C.A., S. C. Olsen and B.J. Hannegan, O. Wild and M.J. Prather (2000),
522 Stratosphere ozone in 3-D models: A simple chemistry and the cross-tropopause flux,
523 *J. Geophys. Res.*, *105(D11)*, 14653-14666, 10.1029/2000JD900124.

524 Michelsen, H. A., G. L. Manney, M. R. Gunson, R. Zander (1998), Correlations of strato-
525 spheric abundances of NO_y, O₃, N₂O, and CH₄ derived from ATMOS measurements,
526 *J. Geophys. Res.*, *103(D21)*, 28347-28360, 10.1029/98JD02850.

527 Michelsen, H. A., G. L. Manney, M. R. Gunson, C. P. Rinsland, R. Zander (1998), Correla-
528 tions of stratospheric abundances of CH₄ and N₂O derived from ATMOS measurements,
529 *Geophys. Res. Lett.*, *25(15)*, 2777-2780, 10.1029/98GL01977.

530 Nassar R., P. F. Bernath, C. D. Boone, G. L. Manney, S. D. McLeod, C. P. Rinsland, R.
531 Skelton, K. A. Walker (2005), Stratospheric abundances of water and methane based on
532 ACE-FTS measurements, *Geophys. Res. Lett.*, *32*, L15S04, doi:10.1029/2005GL022383.

533 Nagatani, R. M., and J. E. Rosenfield, Temperature (1993), net heating and circulation,
534 in *The Atmospheric Effects of Stratospheric Aircraft: Report of the 1992 Models and*
535 *Measurements Workshop, NASA Reft Publ. 1292*, edited by M. J. Prather and E. E.
536 Remsberg, pp. A1-A47.

- 537 Prather, M. (1992), Catastrophic loss of stratospheric ozone in dense volcanic clouds, *J.*
538 *Geophys. Res.*, *97(D9)*, 10,18710,191.
- 539 Prather, Michael and E Rensburg (1993), The atmospheric effects of stratospheric air-
540 craft. Report of the 1992 models and measurements Workshop. *NASA Publ 1292*.
- 541 Prather, M., D. Ehhalt, F. Dentener, R. G. Derwent, E. Dlugokencky, E. Holland, I. S. A.
542 Isaksen, J. Katima, V. Kirchhoff, P. Matson, P. M. Midgley, and M. Wang, Chapter 4
543 (2001), Atmospheric Chemistry and Greenhouse Gases, in *Climate Change 2001: The*
544 *Scientific Basis*, J.T. Houghton et al., eds., *Cambridge U. Press*, pp. 239-287.
- 545 Randel, W. J., and J. B. Cobb (1994), Coherent variations of monthly mean total ozone
546 and lower stratospheric temperature, *J. Geophys. Res.*, *99(D3)*, 54335447.
- 547 Randel, W.J., B.A. Boville, J.C. Gille, P.L. Bailey, S.T. Massie, J.B. Kumer, J.L. Mer-
548 genthaler, and A.E. Rochem (1994), Simulation of Stratospheric N₂O in the NCAR
549 CCM2: Comparison with CLAES Data and Global Budget Analyses. *J. Atmos. Sci.*,
550 *51*, 2834-2845.
- 551 Randel, W.J., and F. Wu, 1996: Isolation of the Ozone QBO in SAGE II Data by Singular-
552 Value Decomposition. *J. Atmos. Sci.*, *53*, 2546-2559.
- 553 Randel W. J., R.S. Stolarski, D.M. Cunnold, J.A. Logan, M. J. Newchurch, and J. M.
554 Zawodny, 1999: Trends in the Vertical Distribution of Ozone, *Science* *285* (5434), 689,
555 DOI:10.1126/science.285.5434.1689.
- 556 Randel W. J., F. Wu (2007), A stratospheric ozone profile data set for 19792005: Variabil-
557 ity, trends, and comparisons with column ozone data, *J. Geophys. Res.*, *112*, D06313,
558 doi:10.1029/2006JD007339.

- 559 Salawitch R. J., D. K. Weisenstein, L. J. Kovalenko, C. E. Sioris, P. O. Wennberg, K.
560 Chance, M. K. W. Ko, C. A. McLinden (2005), Sensitivity of ozone to bromine in the
561 lower stratosphere, *Geophys. Res. Lett.*, *32*, L05811, doi:10.1029/2004GL021504.
- 562 Sander et al. (2006), Chemical kinetics and photochemical data for use in atmospheric
563 studies, Evaluation Number 15. *JPL Publication 06-2.*, Jet Propul. Lab., Pasadena,
564 Calif.
- 565 Schoeberl, M.A. et al. (1993), The evolution of ClO and NO along air parcel trajectories,
566 *Geophys. Res. Lett.*, *20*(22), 2511-2514
- 567 Simmons A., M. Hortal, G. Kelly, A. McNally, A. Untch and S. Uppala (2005), ECMWF
568 analyses and forecasts of stratospheric winter polar vortex breakup: September 2002 in
569 the southern hemisphere and related events. *J. Atmos. Sci.*, *62*, 668-689.
- 570 Stevenson, D. S., et al. (2006), Multimodel ensemble simulations of present-day and near-
571 future tropospheric ozone, *J. Geophys. Res.*, *111*, D08301, doi:10.1029/2005JD006338.
- 572 Stolarski, R.S., A.R. Douglass, S. Steenrod, and S. Pawson (2006), Trends in Stratospheric
573 Ozone: Lessons Learned from a 3D Chemical Transport Model. *J. Atmos. Sci.*, *63*,
574 10281041.
- 575 Strahan, S. E. (1999), Climatologies of lower stratospheric NO_y and O₃ and correlations
576 with N₂O based on in situ observations, *J. Geophys. Res.*, *104*(D23), 30463-30480,
577 10.1029/1999JD900775.
- 578 Sudo, K., M. Takahashi, and H. Akimoto (2003), Future changes in stratosphere-
579 troposphere exchange and their impacts on future tropospheric ozone simulations, *Geo-*
580 *phys. Res. Lett.*, *30*(24), 2256, doi:10.1029/2003GL018526.

- 581 Thomason, L. W., L. R. Poole, and T. Deshler (1997), A global climatology of strato-
582 spheric aerosol surface area density deduced from Stratospheric Aerosol and Gas Ex-
583 periment II measurements: 1984-1994, *J. Geophys. Res.*, 102(D7), 8967-8976.
- 584 Thompson, D. W. J., and J. M. Wallace, 1998: The Arctic Oscillation signature in the
585 wintertime geopotential height and temperature fields. *Geophys. Res. Lett.*, 25, No. 9,
586 1297-1300.
- 587 Thornton, B. F. et al. (2005), Variability of active chlorine in the lowermost Arctic strato-
588 sphere, *J. Geophys. Res.*, 110(D22), D22304.
- 589 Thuillier, G., L. Floyd, T. N. Woods, R. Cebula, E. Hilsenrath, M. Herse, D. Labs (2004),
590 Solar Irradiance Spectra for Two Solar Activity Levels, *Adv. Space Res.*, 34, 256-261.
- 591 Wamsley, P. R., et al. (1998), Distribution of halon-1211 in the upper troposphere and
592 lower stratosphere and the 1994 total bromine budget, *J. Geophys. Res.*, 103(D1), 1513-
593 1526.
- 594 Wild, O., J. K. Sundet, M. J. Prather, I. S. A. Isaksen, H. Akimoto, E. V. Browell,
595 and S. J. Oltmans (2003), Chemical transport model ozone simulations for spring
596 2001 over the western Pacific: Comparisons with TRACE-P lidar, ozonesondes, and
597 Total Ozone Mapping Spectrometer columns, *J. Geophys. Res.*, 108(D21), 8826,
598 doi:10.1029/2002JD003283.
- 599 WMO (World Meteorological Organization), Scientific Assessment of Ozone Depletion:
600 2006, *Global Ozone Research and Monitoring Project Report No. 50*, 572 pp., Geneva,
601 Switzerland, 2007.
- 602 Woodbridge, E. L., et al. (1995), Estimates of total organic and inorganic chlorine in the
603 lower stratosphere from in situ and flask measurements during AASE II, *J. Geophys.*

604 *Res.*, 100(D2), 3057-3064.

605 Ziemke, J.R. and S. Chandra (2003), La Nina and El Nino- induced variabilities of ozone
606 in the tropical lower atmosphere during 1970-2001, *Geophys. Res. Lett.*, 30(3), 1142,
607 doi:10.1029/2002GL016387.

608 Ziemke, J. R., S. Chandra, B. N. Duncan, L. Froidevaux, P. K. Bhartia, P. F. Levelt, and
609 J. W. Waters (2006), Tropospheric ozone determined from Aura OMI and MLS: Evalu-
610 ation of measurements and comparison with the Global Modeling Initiative's Chemical
611 Transport Model, *J. Geophys. Res.*, 111, D19303, doi:10.1029/2006JD007089.

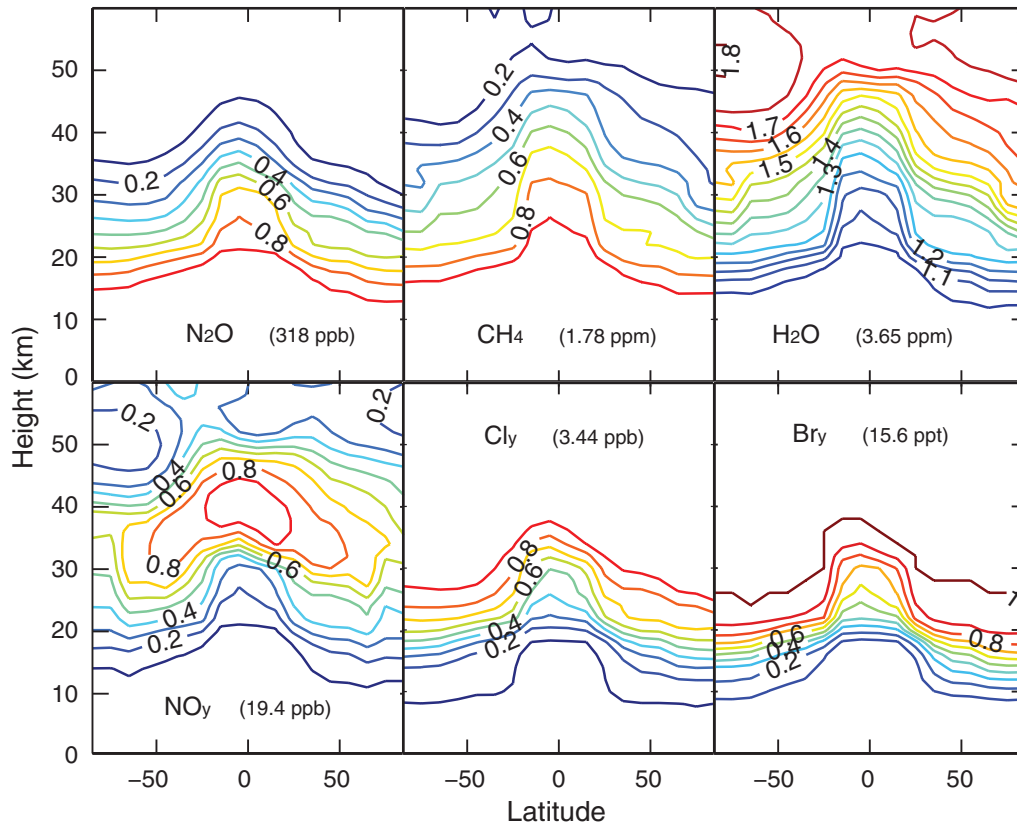


Figure 1. The Linz climatologies of trace gases for January. For N_2O and CH_4 the patterns are normalized relative to their mean tropospheric abundances; and for H_2O , to the tropopause value. The trace gas families (NO_y , Cl_y , Br_y) are normalized relative to their maximum values (in the upper stratosphere). For year 2004, the normalization values are noted.

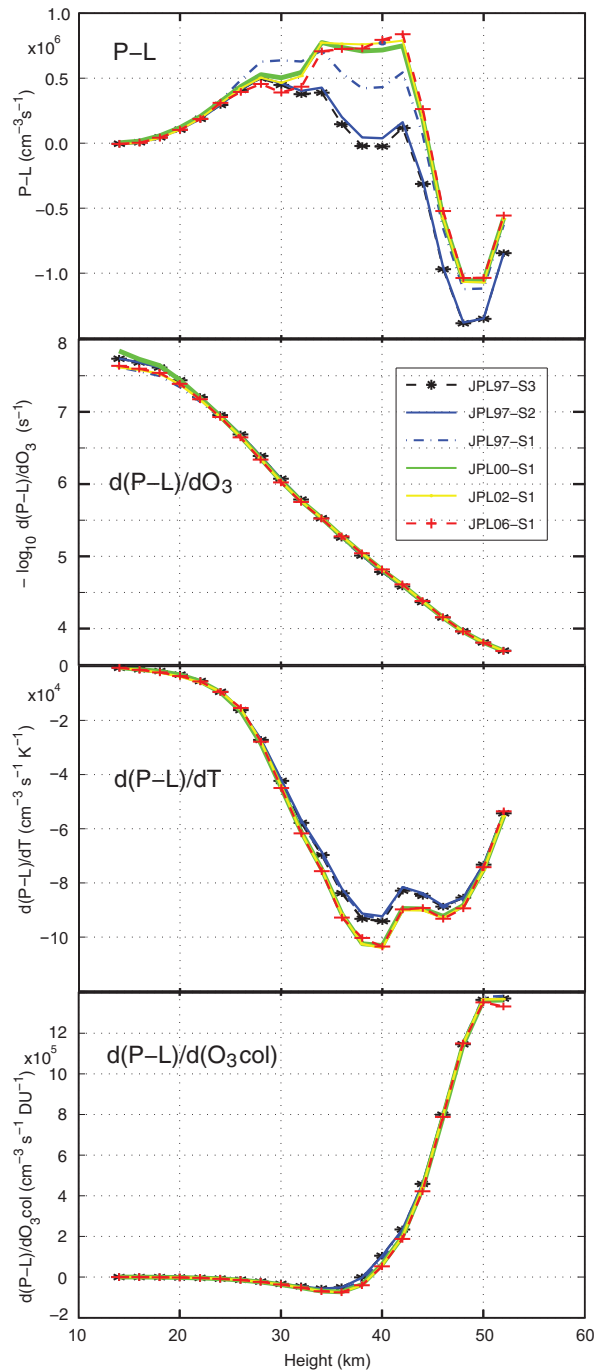


Figure 2. The sensitivity of Lincoz terms (Equation 1) to different radiation and chemical updates using the standard ATMOS-profile on May 31 at 30N as the basic state. See the text for details.

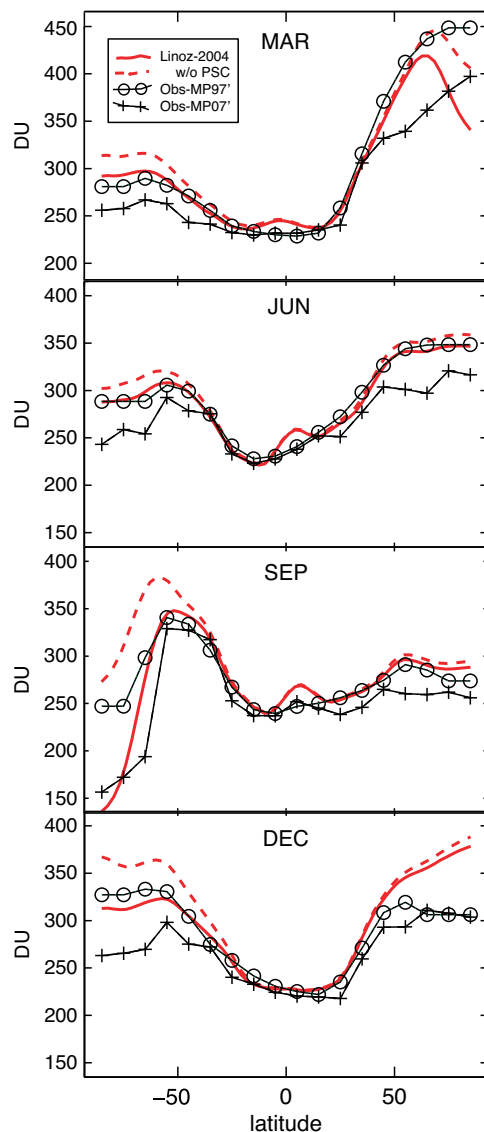


Figure 3. Stratospheric column O₃ (DU) as a function of latitude for March, June, September and December. The stratospheric column is integrated over the atmosphere where O₃ > 100 ppb. The four different profiles are: climatology compiled by McPeters et al. (1997) (black line with o); climatology compiled by McPeters et al. (2007) (black line with +); Simulation with Linoz-2004 in the UCI CTM with the 1997 ECMWF IFS met data (red solid line); the same Linoz-2004 simulation but without PSC parameterization (red dashed). See the text for details.

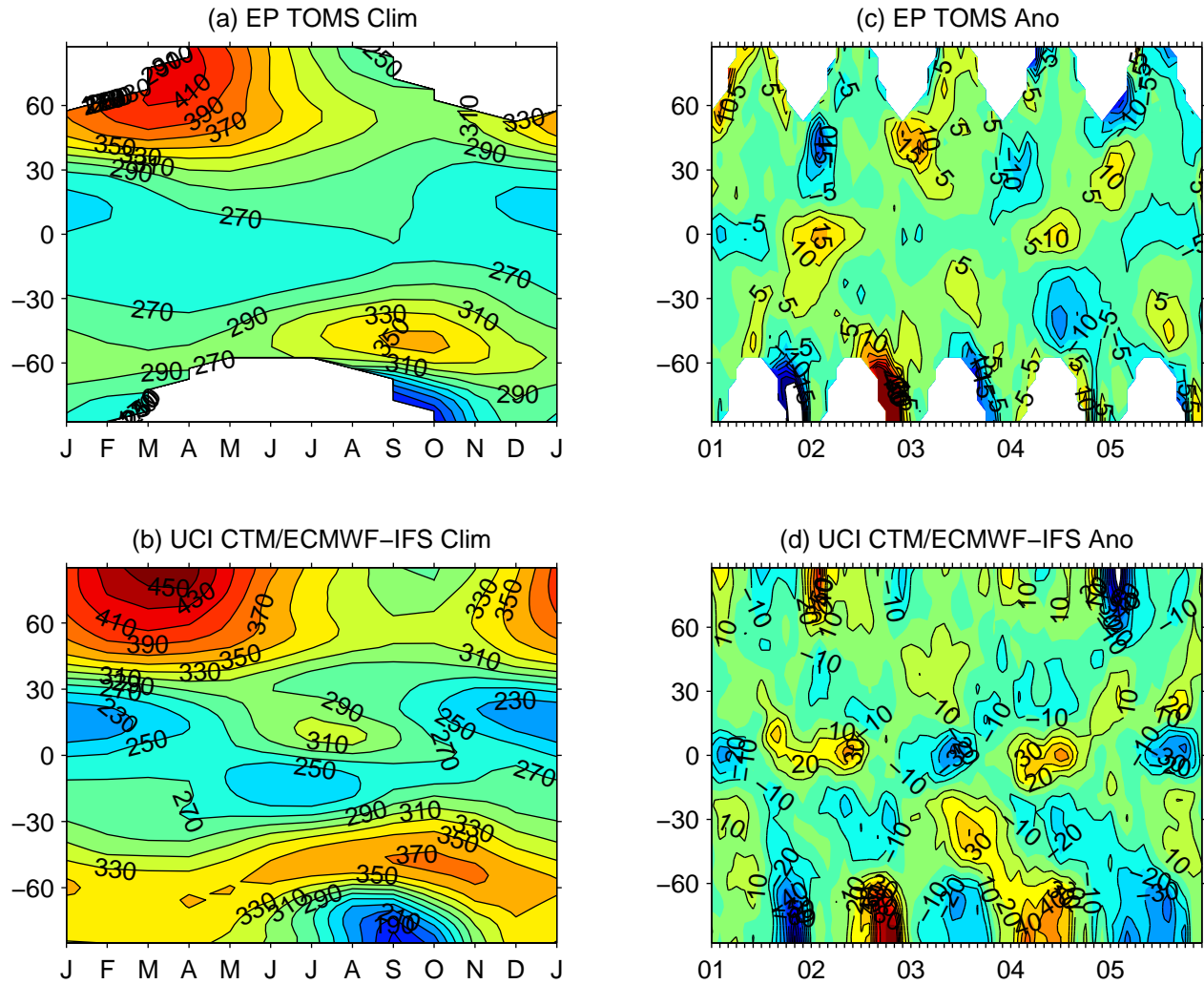


Figure 4. Five-year (2001-2005) monthly zonal-mean climatology of total column O₃ (DU) as a function of latitude and for (a) corrected Earth Probe TOMS and (b) Linoz-2004 CTM simulation using Oslo/EC meteorological data at T42L40 resolution from IFS Cycle 29r2. The anomalies relative to these climatologies from Jan 2001 to Dec 2005 are shown for (c) TOMS and (d) CTM. Contour intervals for the CTM simulation anomalies are 10 DU, but those for the TOMS anomalies are only 5 DU.

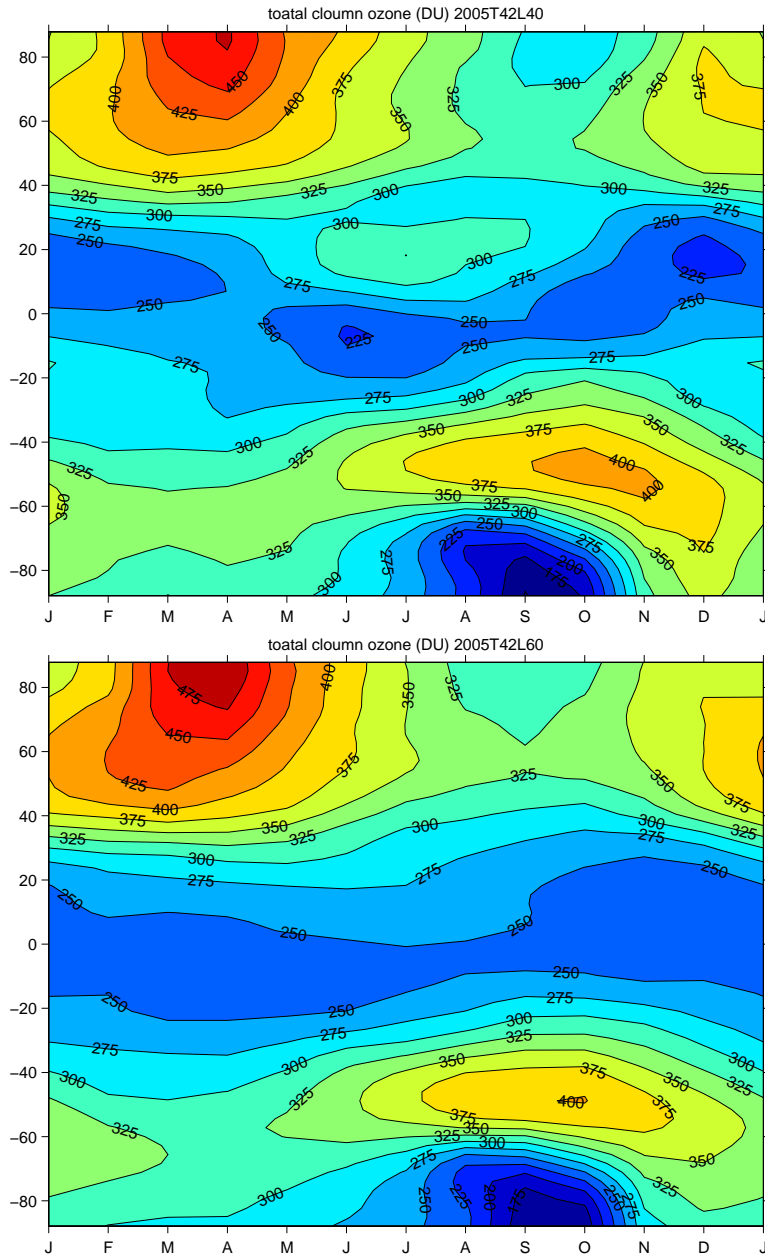


Figure 5. Year 2005 monthly zonal mean total column O_3 (DU) simulated with Linoz-2004 for (top) T42L40 CTM and (bottom) T42L60 CTM.

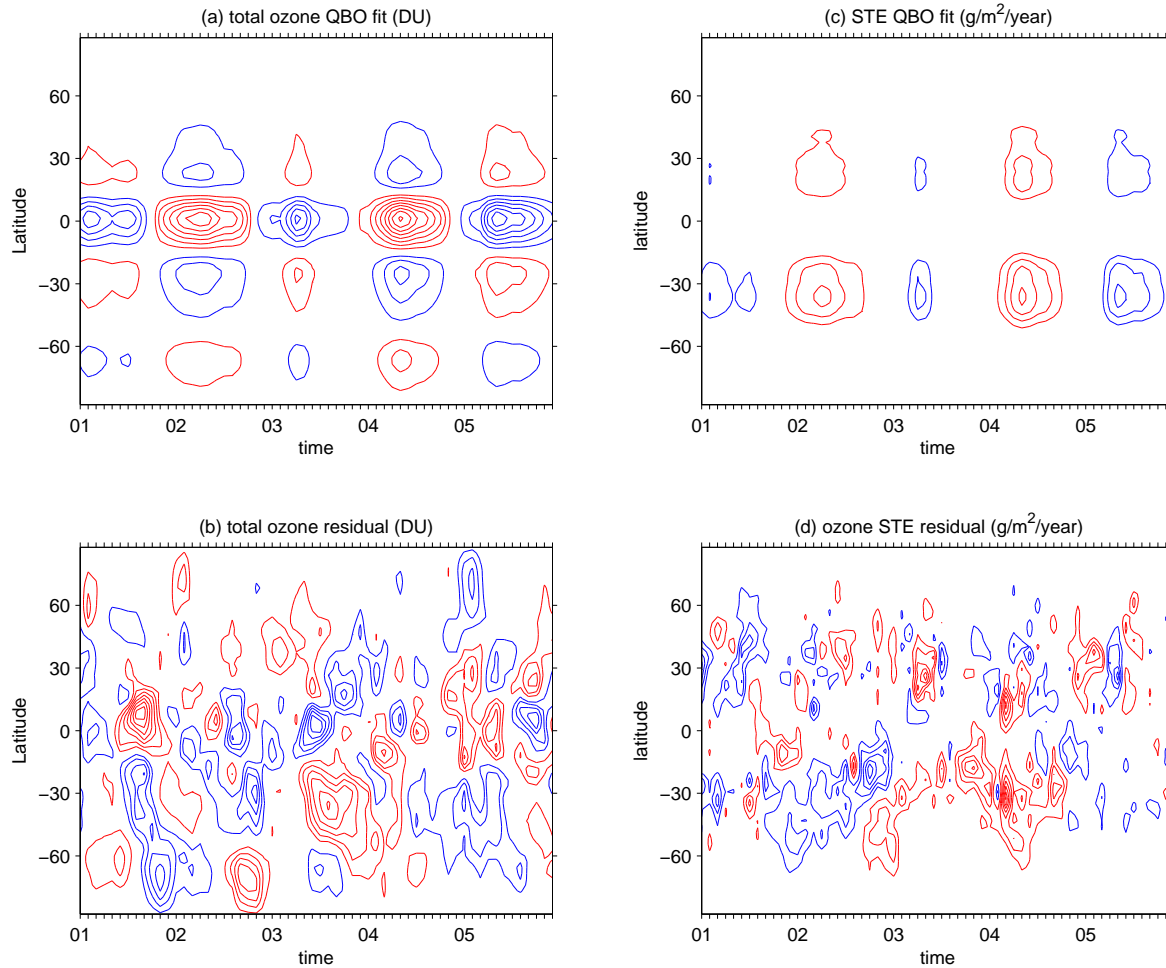


Figure 6. Monthly zonal mean anomalies in the modeled total column O_3 split into (a) QBO signal and (b) residuals, taken from the 2001-2005 simulation shown in Fig. 4d. Contour intervals are +5, +10, +15, DU (solid red) and -5, -10, -15, (dashed blue). Corresponding monthly zonal mean anomalies in the STE O_3 fluxes are shown for (c) QBO signal with contour intervals of $\pm 0.05 \text{ g m}^{-2} \text{ yr}^{-1}$ and (d) the residuals with contour intervals of $\pm 0.10 \text{ g m}^{-2} \text{ yr}^{-1}$. Zero contour lines are omitted.

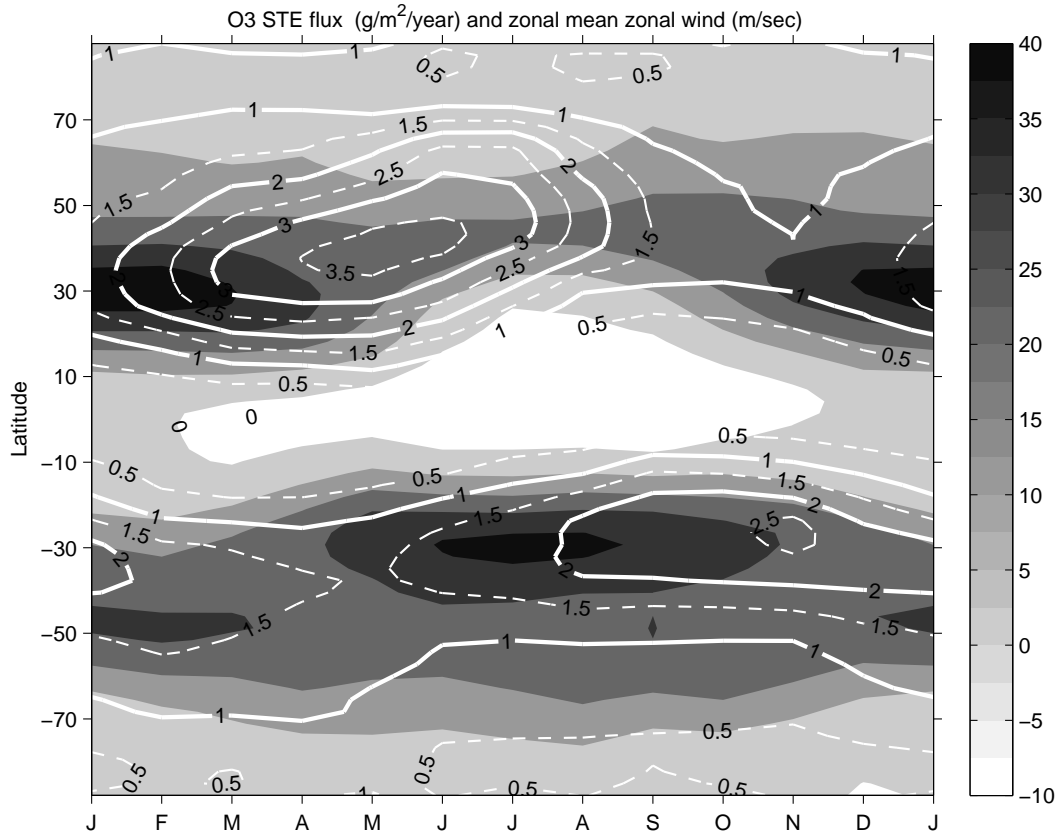


Figure 7. Latitude by month average STE O₃ fluxes (white-line contours at 0 to +3.5 g m⁻² yr⁻¹) from UCI CTM with Linoz-2004 driven by ECMWF IFS T42L40 2001-2005 met data. Zonal-mean zonal wind at 200 hPa (grey-scale contours at -5, +5, +15, +25, +35 ms⁻¹) from the same meteorological data.

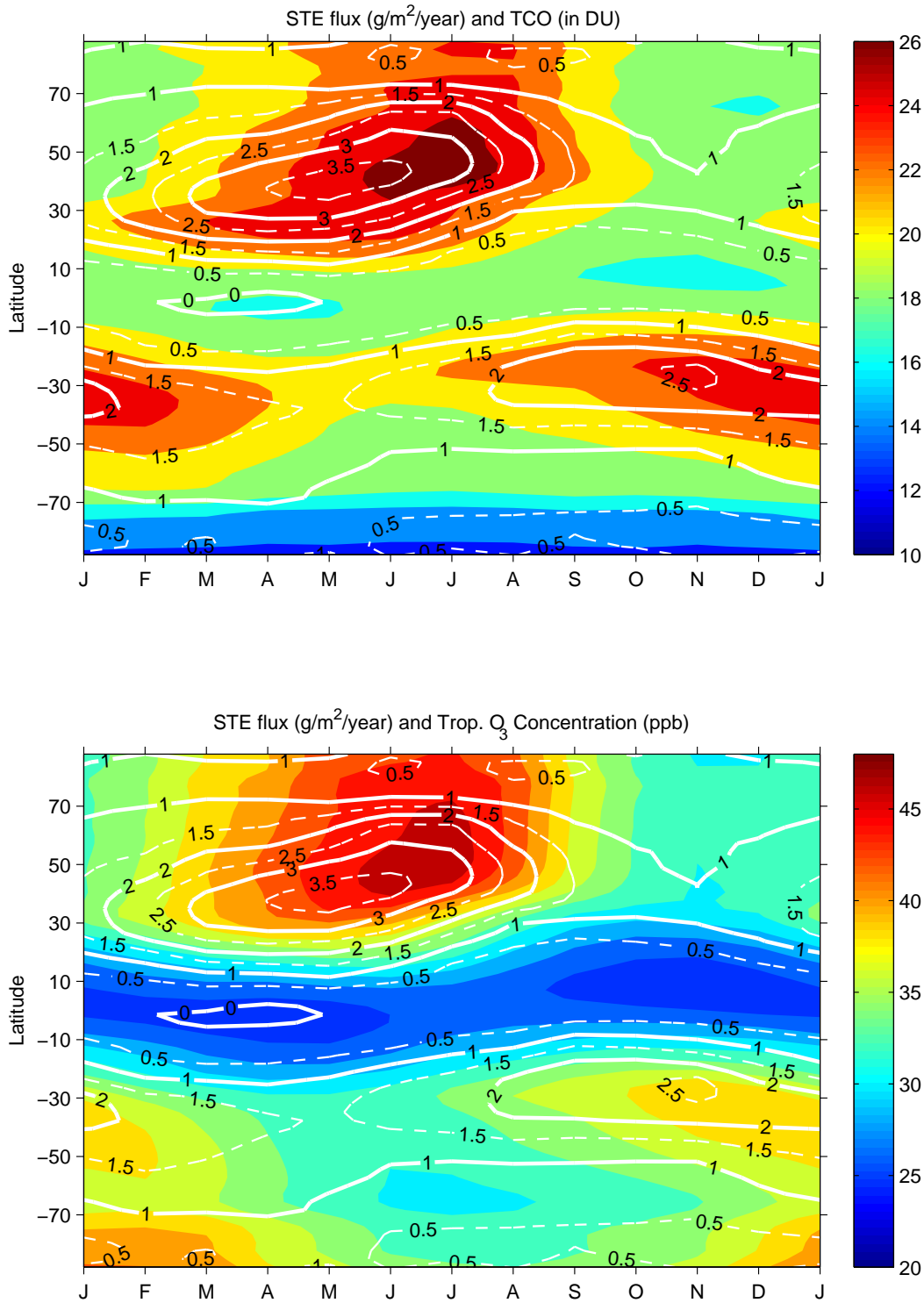


Figure 8. (top) Latitude by month average STE O₃ fluxes (see Fig 7) on top of simulated tropospheric column ozone (TCO, color-filled contour interval, 2 DU) for Linoz-2004 simulations. (bottom) Same STE O₃ fluxes on top of monthly zonal-mean tropospheric O₃ abundance (ppb) with color-filled contours interval, 2 ppb.

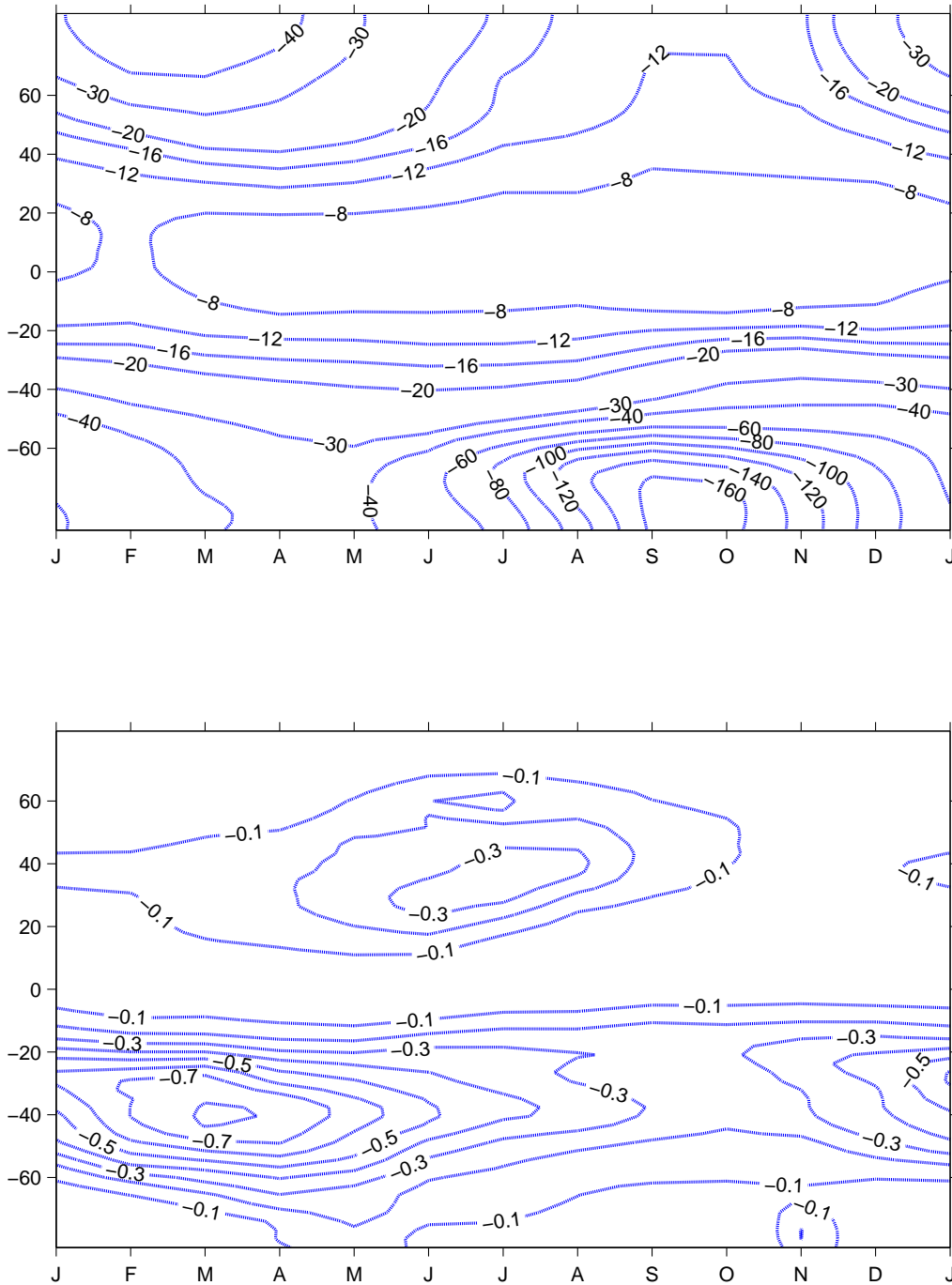


Figure 9. (top) Monthly zonal-mean differences in total column O₃ (DU) for Linoz-2004BrT minus Linoz-1979Br. Both Linoz simulations are driven by the same 5-year ECMWF IFS data from 2001-2005. (bottom) Differences in STE O₃ flux (g m⁻² yr⁻¹) for Linoz-2004BrT minus Linoz-1979Br.

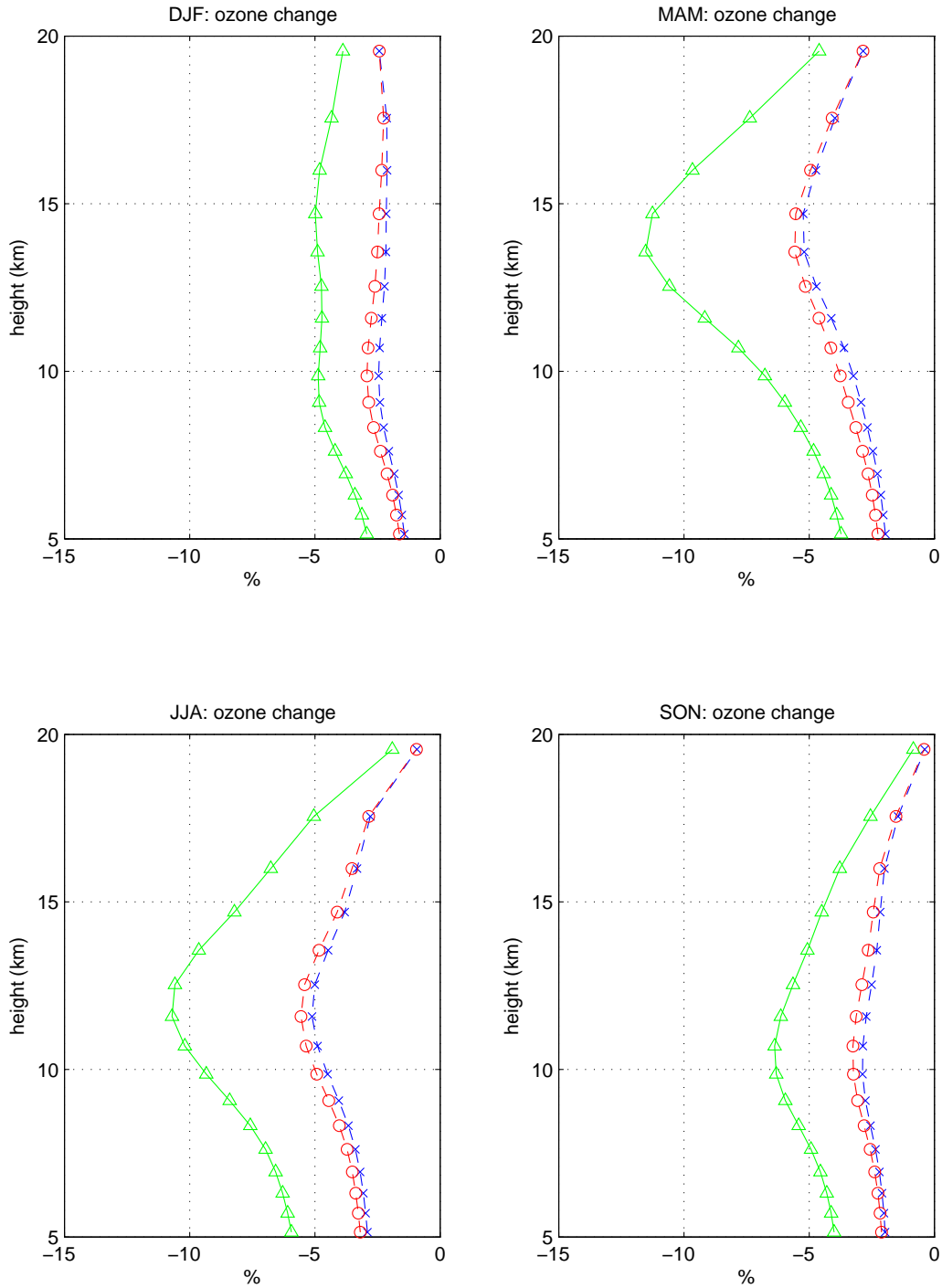


Figure 10. Seasonal profile changes in O₃ abundance (%) over the lower stratosphere and upper troposphere at 40N-50N for all Linoz-2004 runs minus their respective pre-ozone depletion runs. Linoz-2004 minus Linoz-1979 (crosses), Linoz-2004Br-Linoz-1979Br (circles) and Linoz-2004BrT minus Linoz-1979Br (triangles). All calculations use the same meteorological data.

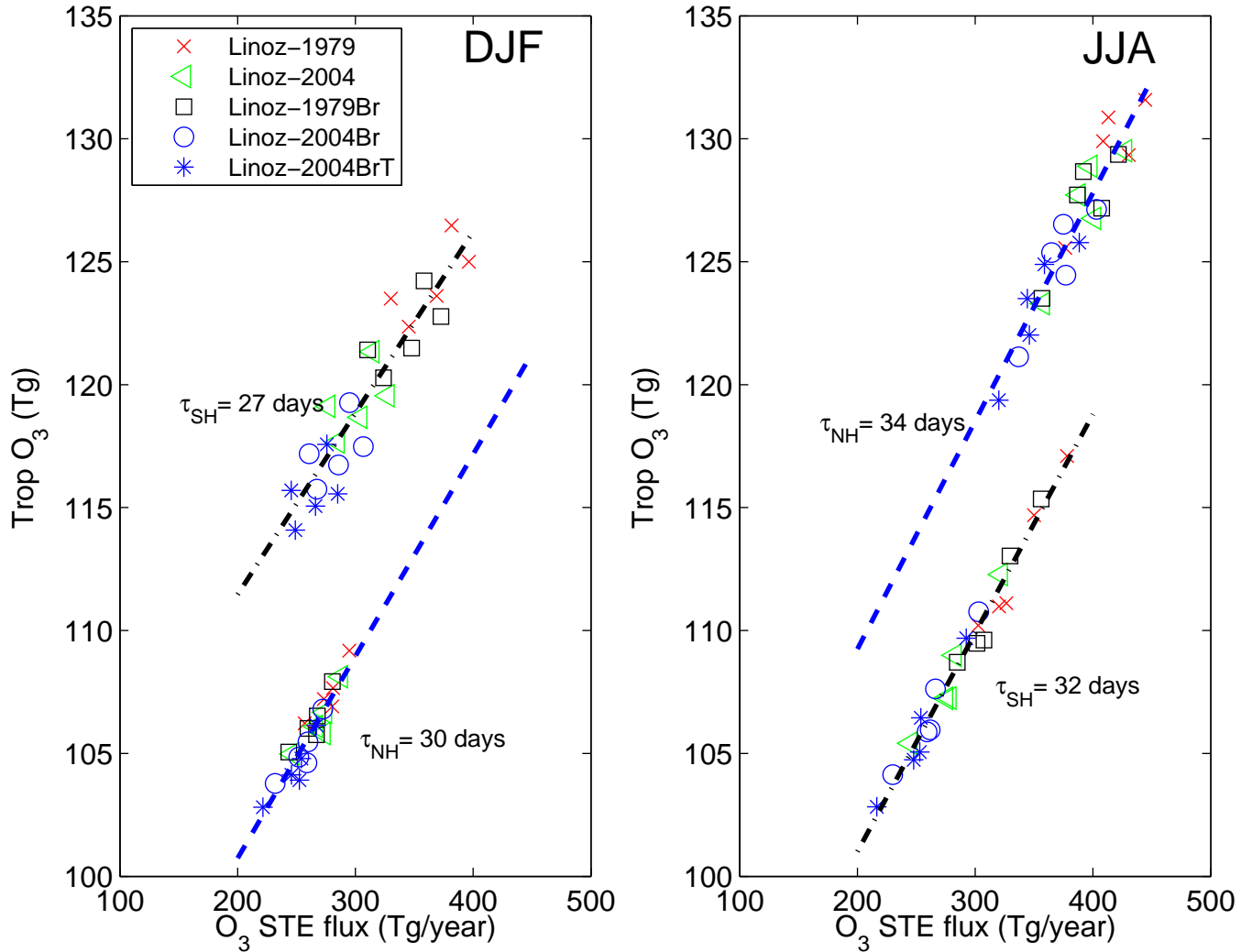


Figure 11. Mean tropospheric O₃ (Tg) vs. STE O₃ flux (Tg/yr) by hemisphere for DJF and JJA. The linear regression fit is shown in dashed blue line for the NH and black dashed-dot line for the SH. The slopes indicate the lifetimes of the perturbations to tropospheric ozone and are labelled in unit of days. The five different Linoz models are labeled with symbols: -1979 (red crosses), -1979Br (black squares), -2004 (green left-triangles), -2004Br (blue circles), and -2004BrT (blue asterisks).

| Species abundances\Linnoz v2 | Linnoz-1979 | Linnoz-2004 | Linnoz-1979Br | Linnoz-2004Br | Linnoz-2004BrT |
|------------------------------|-------------|-------------|---------------|---------------|----------------|
| N ₂ O (ppbv) | 300.4 | 318.4 | 300.4 | 318.4 | 318.4 |
| NO _y (ppbv) | 18.2 | 19.4 | 18.2 | 19.4 | 19.4 |
| Cl _y (pptv) | 2242 | 3437 | 2242. | 3437 | 3437 |
| Br _y (pptv) | 8.7 | 15.6 | 14.7 | 21.6 | 21.6 |
| CH ₄ (ppbv) | 1555 | 1777 | 1555 | 1777 | 1777 |
| H ₂ O (ppmv) | 3.65 | 3.65 | 3.65 | 3.65 | 3.65 |
| PSC activa. Temp (K) | N. A. | 195 | N. A. | 195 | 199 |

Table 1. Prescribed abundances of long-lived species and activation temperatures for the PSC parameterization used for deriving the 5 Linnoz tables indicated in the column headings. Note that the PSC parameterization is not used for pre-ozone depletion runs (Linnoz-1979 and Linnoz-1979Br). See text for details.